JCTC Journal of Chemical Theory and Computation

Article

pubs.acs.org/JCTC

Anchor Points Reactive Potential for Bond-Breaking Reactions

Ke R. Yang, Xuefei Xu, and Donald G. Truhlar*

Department of Chemistry, Chemical Theory Center, and Supercomputing Institute, University of Minnesota, Minneapolis, Minnesota 55455-0431 United States

Supporting Information

ABSTRACT: We present a new method for fitting potential energy surfaces in molecular-mechanics-like internal coordinates based on data from electronic structure calculations. The method should be applicable to chemical reactions involving either bond dissociation or isomerization and is illustrated here for bond dissociation, in particular the breaking of an O−H bond in methanol and the breaking of an N−H bond in dimethylamine. As compared to previously available systematic methods for fitting global potential energy surfaces, it extends the maximum size of the system than can be treated by at least an order of magnitude.

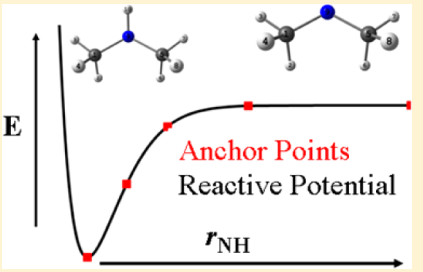

1. INTRODUCTION

Potential energy surfaces (PESs) and their associated force fields play critical roles in chemical reactions and molecular interactions; the construction of a PES is the first step in computing the dynamics[1−4] or optimizing a geometry. The PES may be implicit, as in direct dynamics, or explicit, when an analytical PES is available. Molecular mechanics (MM), which denotes an analytical potential expressed in internal coordinates, is perhaps the simplest way to construct a PES, but conventional MM omits cross terms and is valid only near an equilibrium structure. Nevertheless MM finds a myriad of uses and is widely used in the study of protein folding, drug docking, and materials simulations. Many MM force fields, for instance, CHARMM,[5−8] AMBER,[9−13] GROMOS,[14] MM3,[15−17] OPLS,[18−20] UFF,[21] MMFF94,[22−25] GAFF,[26] and TraPPE,[27,28] have been developed for the study of biopolymers, other polymers, and small organic molecules. The key advantage of popular MM force fields is that they involve transferable parameters that need not be redetermined for each new molecule studied. Recently, MM-like force fields for specific molecules based on quantum mechanical electronic structure calculations of energies and Hessians at an equilibrium structure have been developed for more accurate simulations.[29,30] However, one of the limitations of even such molecule-specific internal-coordinate force fields is their inability to describe bond-breaking processes.

Recent development in potential energy surface fitting such as using global permutationally invariant polynomials[31,32] and the interpolated moving least-squares (IMSL) method,[33−35] can describe bond breaking processes and have been used successfully to generate global potential energy surfaces based on electronic structure calculations, but they require many such calculations. In particular, the number of electronic calculations required for PES fitting grows rapidly with the dimensionality of the system, and therefore, most fitted PESs are limited to systems with five or fewer atoms. For a system with N atoms, the number of internal degrees of freedom is $F = 3N - 6$, and the number of data points grows as m^F, where m is the number of points needed to span a given degree of freedom. For a molecule with only ten atoms, using only four points in each dimension for the fit still requires $4^{24} \cong 10^{14}$ data points.

Conventional MM can be extended to include bond breaking by substituting a Morse curve or similar one-dimensional potential energy curve for the usual bond stretching term, but this does not allow for the change in geometrical parameters and force constants in other modes as the breaking bond is extended, and so, it can be very inaccurate. Some work has been carried out to extend MM to bond breaking processes without assuming such separability of the bond breaking coordinate, but still allowing for the possibility of using general or specific-range parameters, as in the reactive empirical bond order method,[36,37] ReaXFF,[38,39] or the valence bond order (VBO) method,[40] but such methods have less accuracy for global or semiglobal PESs than conventional MM has near equilibrium structures. It would be desirable to combine analytical potentials in internal coordinates for degrees of freedom that involve small distortions from equilibrium structures with model potentials based on general functional forms to fit degrees of freedom involved in or closely coupled to bond breaking. Such an approach would be analogous to the combined quantum mechanics/molecular mechanics (QM/MM) method where MM is used for degrees of freedom of spectator atoms, and QM is used for degrees of freedom of active ones. Unlike QM/MM, which has been used widely for incorporating MM into electronic structure calculations of PESs of large systems such as enzymes and catalysis,[41−47] very few studies have been performed that incorporate MM-like force fields into the fitting of high-dimensional PESs.[48] In this article, we present a method called anchor points reactive potential (APRP) that combines fitting of quantum mechanical potential energy surfaces for selected degrees of freedom with molecule-specific MM-like

Received: December 12, 2013

   dx.doi.org/10.1021/ct401074s | J. Chem. Theory Comput. XXXX, XXX, XXX−XXX

force fields for other degrees of freedom to obtain a high-dimensional PES to treat bond-breaking processes.

2. METHODOLOGY

2.1. Anchor Points Reactive Potential (APRP) Method. Conventional molecular mechanics force fields cannot describe chemical reactions in which bond breaking processes are involved. In our proposed anchor points reactive potential method, the contributions to a potential energy surface (PES) are divided according to their dependence on three predefined groups of internal coordinates:

1. Reaction coordinates: $\mathbf{q}$
2. Secondary coordinates: $\mathbf{s}$
3. Tertiary coordinates: $\mathbf{Q}$

The potential energy is written as

$$V = V^{[1]}(\mathbf{q}) + V^{[2]}(\mathbf{s}|\mathbf{q}) + V^{[3]}(\mathbf{Q}|\mathbf{q}) \tag{1}$$

where $f(x|y)$ denotes a function with a dependence on x and a parametric dependence on y. The three terms in eq 1 will be called the primary, secondary, and tertiary potentials; the primary and secondary terms can be completely general. In the present application, the reaction coordinate group consists of a single bond length r, and we will present the equations in the present subsection for this single-reaction-coordinate case to make the ideas more clear. To fit $V^{[2]}(\mathbf{s}|r)$ and $V^{[1]}(r)$, we need to calculate many data points in the space of $\mathbf{s}$ and r for a set of fixed values of the tertiary coordinates corresponding to a reference structure, and for the calculation of the torsional term in the secondary potential, we also calculate a grid of energies in a two-dimensional subspace with the other coordinates relaxed (see further details below).

The tertiary potential is described by analytic potentials in internal displacement coordinates $\mathbf{Q}^{[a]}$ relative to a set of anchor structures a with the anchor structures spaced along the reaction coordinates at a set of anchor values $\{r_a = r_i, i = 1, 2, ..., N_A\}$:

$$V^{[3]}(\mathbf{Q}|r) = \sum_{a=1}^{N_A} V_a(\mathbf{Q}^{[a]}) T_a(r) \tag{2}$$

In eq 2, N_A is the number of anchor structures, $V_a(\mathbf{Q}^{[a]})$ is a molecular mechanics-like potential with molecule-specific and anchor-point-specific parameters at anchor structure a, and $T_a(r)$ is called a tent function. The tent function is defined by

$$T_1(r) \to \begin{cases} 1 & r < r_1 \\ \dfrac{(r - r_2)^4}{(r - r_2)^4 + (r - r_1)^4} & r_1 \le r < r_2 \end{cases} \tag{3a}$$

$$T_a(r) \to \begin{cases} \dfrac{(r - r_{a-1})^4}{(r - r_a)^4 + (r - r_{a-1})^4} & r_{a-1} \le r < r_a \\ \dfrac{(r - r_{a+1})^4}{(r - r_{a+1})^4 + (r - r_a)^4} & r_a \le r < r_{a+1} \end{cases}$$
$$\text{for} \quad a = 2, ..., N_A - 1 \tag{3b}$$

$$T_{N_A}(r) \to \begin{cases} \dfrac{(r - r_{N_A-1})^4}{(r - r_{N_A})^4 + (r - r_{N_A-1})^4} & r_{N_A-1} \le r < r_{N_A} \\ 1 & r_{N_A} \le r \end{cases} \tag{3c}$$

Tertiary coordinates $\mathbf{Q}$ are further divided into two subgroups: stiff coordinates $\mathbf{Q}_{\text{stiff}}$ such as stretches, bends, and rigid torsions, and soft torsion coordinates $\mathbf{Q}_{\text{ST}}$, which involve wide-amplitude motion. The tertiary potential at anchor structure a is written as

$$V_a(\mathbf{Q}^{[a]}) = V_a^{\text{stiff}}(\mathbf{Q}_{\text{stiff}}^{[a]}) + V_a^{\text{ST}}(\mathbf{Q}_{\text{ST}}^{[a]}) \tag{4}$$

where $V_a^{\text{stiff}}(\mathbf{Q}_{\text{stiff}}^{[a]})$ is the potential energy contribution from stiff coordinates, and $V_a^{\text{ST}}(\mathbf{Q}_{\text{ST}}^{[a]})$ is the potential energy contribution from soft torsions.

Partial optimization is performed for each anchor structure a, with the only constraint being $r = r_a$, and the force constant matrix $\mathbf{F}^{[a]}$ in internal displacement coordinates is calculated for the optimized structure. Element i of the stiff internal displacement coordinate vector $\mathbf{Q}_{\text{stiff}}^{[a]}$ is defined as

$$Q_{\text{stiff},i}^{[a]} = S_i - S_{i,e}^{[a]} \tag{5}$$

where S_i is an internal coordinate, and $S_{i,e}^{[a]}$ is the optimized value of S_i in the constrained optimized geometry of anchor point a.

Since $V^{[2]}(\mathbf{s}|\mathbf{q})$ and $V^{[1]}(\mathbf{q})$ are fitted to data corresponding to a rigid tertiary subspace corresponding to a reference structure, while the tertiary potential is expanded at partially optimized anchor structure a, a relaxation energy $V^{[a]}$ needs to be considered; this is defined as the energy difference between partially optimized anchor structure a and the rigid geometry with the same r_a. Then, $V_a^{\text{stiff}}(\mathbf{Q}_{\text{stiff}}^{[a]})$ is expanded near anchor structure a as

$$V_a^{\text{stiff}}(\mathbf{Q}_{\text{stiff}}^{[a]}) = V^{[a]} + \frac{1}{2}\mathbf{Q}_{\text{stiff}}^{[a]T}\mathbf{F}_{\text{stiff}}^{[a]}\mathbf{Q}_{\text{stiff}}^{[a]} \tag{6}$$

where $\mathbf{F}_{\text{stiff}}^{[a]}$ is the partial force constant matrix in the stiff subspace. The other tertiary potential term is parametrized as

$$V_a^{\text{ST}}(\mathbf{Q}_{\text{ST}}^{[a]}) = \sum_{\tau=1}^{N_{\text{ST}}} V_\tau^{[a]}[1 - \cos n_\tau(\varphi_\tau - \varphi_{\tau,e}^{[a]})] \tag{7}$$

where N_{ST} is the number of soft torsions, n_τ is the local periodicity of the torsion, and $V_\tau^{[a]}$ and $\varphi_{\tau,e}^{[a]}$ are respectively the torsion barrier and equilibrium torsion angle for torsion τ at anchor structure a.

2.2. Analytical Cartesian Gradient. In order to perform efficient dynamic studies, we require analytic Cartesian gradients of the PES. Denoting a column vector containing $3N$ Cartesian coordinates ($\xi_{3i-2} = x_i$, $\xi_{3i-1} = y_i$, $\xi_{3i} = z_i$, $i = 1, ..., N$, where N is the number of atoms) as $\boldsymbol{\xi}$, eq 1 yields

$$\frac{dV}{d\boldsymbol{\xi}} = \frac{dV^{[1]}(\mathbf{q})}{d\boldsymbol{\xi}} + \frac{dV^{[2]}(\mathbf{s}|\mathbf{q})}{d\boldsymbol{\xi}} + \frac{dV^{[3]}(\mathbf{Q}|\mathbf{q})}{d\boldsymbol{\xi}} \tag{8}$$

Each term in eq 8 is constructed with internal coordinates, so the chain rule must be applied to obtain the analytic Cartesian gradient. This yields

dx.doi.org/10.1021/ct401074s | J. Chem. Theory Comput. XXXX, XXX, XXX−XXX

$$\frac{dV}{d\xi} = \left(\frac{\partial V^{[1]}(\mathbf{q})}{\partial \mathbf{q}} + \frac{\partial V^{[2]}(\mathbf{s}|\mathbf{q})}{\partial \mathbf{q}} + \frac{\partial V^{[3]}(\mathbf{Q}|\mathbf{q})}{\partial \mathbf{q}} \right) \frac{\partial \mathbf{q}}{\partial \xi} + \frac{\partial V^{[2]}(\mathbf{s}|\mathbf{q})}{\partial \mathbf{s}} \frac{\partial \mathbf{s}}{\partial \xi} + \frac{\partial V^{[3]}(\mathbf{Q}|\mathbf{q})}{\partial \mathbf{Q}} \frac{\partial \mathbf{Q}}{\partial \xi} \quad (9)$$

For the APRP PES of eq 1, $(\partial V^{[1]}(\mathbf{q})/\partial \mathbf{q})$, $(\partial V^{[2]}(\mathbf{s}|\mathbf{q})/\partial \mathbf{q})$, $(\partial V^{[3]}(\mathbf{Q}|\mathbf{q})/\partial \mathbf{q})$, $(\partial V^{[2]}(\mathbf{s}|\mathbf{q})/\partial \mathbf{s})$, and $(\partial V^{[3]}(\mathbf{Q}|\mathbf{q})/\partial \mathbf{Q})$ can be evaluated straightforwardly. The other derivatives,$(\partial \mathbf{q}/\partial \boldsymbol{\xi})$, $(\partial \mathbf{s}/\partial \boldsymbol{\xi})$, and $(\partial \mathbf{Q}/\partial \boldsymbol{\xi})$, are Wilson's rectangular B matrices[49] for reaction, secondary, and tertiary coordinates, with dimensions of $N_q \times 3N$, $N_s \times 3N$, and $N_Q \times 3N$, where N_q, N_s, and N_Q are the number of reaction, secondary, and tertiary coordinates, and they can be evaluated analytically.[50,51]

3. RESULTS AND DISCUSSION

We provide two examples to illustrate the APRP method, namely the O−H dissociation in CH_3OH and the N−H

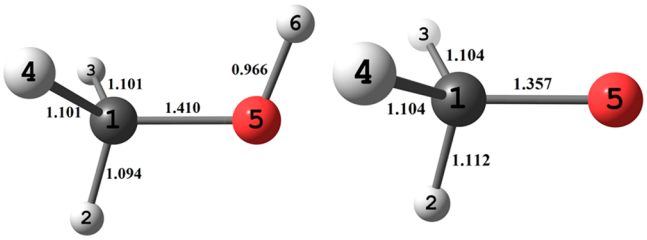

Figure 1. Geometries of CH_3OH (left) and CH_3O (right) (both in C_s symmetry).

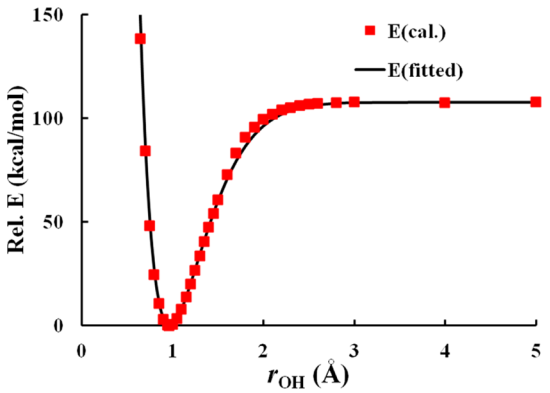

Figure 2. Varshni potential to describe the O−H bond dissociation in CH_3OH. All internal coordinates except the O−H bond distance are held constant along the path used for this figure.

dissociation in $(H_3C)_2NH$. The electronic structure calculations for geometry optimization and energy and force constant calculations were performed with the unrestricted Kohn−Sham formalism with *Gaussian 09*.[52] The M06 exchange−correlation functional[53] and the 6-31+G(d) basis set[54] were used. For integrations to compute the exchange-correlation energy, we used a pruned (99,590) grid [called the ultrafine grid] for all single-point energy calculations and a (150,974) grid [called the superfinegrid] for optimizations and force constant calculations.

3.1. $CH_3OH \rightarrow CH_3O + H$. The reference structure for the parametrization of the primary and secondary potentials is taken to be the equilibrium geometry of CH_3OH. The CH_3OH molecule possesses C_s symmetry. When the H atom is removed, the CH_3O radical undergoes Jahn−Teller distortion from C_{3v} symmetry to C_s symmetry.[55] The optimized geometries and atomic labeling are shown in Figure 1. To treat the O−H bond dissociation, the O−H distance ($r_{OH} = r_{56}$) was chosen as the reaction coordinate; the bending and torsional coordinates that involve the separating H atom ($\theta_{HOC} = \theta_{651}$ and $\varphi_{HOCH} = \varphi_{6512}$), were chosen as secondary coordinates; and the other coordinates are tertiary ($r_{CH} = r_{12}$, r_{13}, r_{14}, $r_{CO} = r_{15}$, $\theta_{HCH} = \theta_{213}$, θ_{214}, θ_{314}, and $\theta_{HCO} = \theta_{215}$, θ_{315}, and θ_{415}) were chosen as tertiary coordinates.

The Varshni model potential, given by

$$V^{[1]}(r_{OH}) = D_1\{1 - (r_1/r_{OH})\exp[-\beta_1((r_1/r_{OH})^2 - 1)]\}^2 \quad (10)$$

was used to fit the O−H dissociation curve in CH_3OH since it has been shown to provide better approximations than the widely used Morse model in diatomics[56,57] and in the C−H dissociation of CH_4.[58] The optimized parameters are given in the Supporting Information, and the calculated and fitted O−H dissociation curves are shown in Figure 2. The H−O−C bending and H−O−C−H torsion in secondary coordinates both involve the dissociated H atom, so they were parametrized with flexible functional forms that depend parametrically on the O−H bond length.

A scan was performed for $r = 0.65$−4.0 Å and $\theta = 60$−$180°$ with other internal coordinates of the equilibrium structure held rigid; the scan showed that at least a cubic term is needed to account for anharmonicity, so we used

$$V^{[2]}_{bend}(\theta|r) = k_2(r)[\cos\theta - \cos\theta_0(r)]^2 + k_3(r)[\cos\theta - \cos\theta_0(r)]^3 \quad (11)$$

Notice that eq 11 has physically correct behavior in the vicinity of $\theta = 180°$, whereas a polynomial in θ rather than cos θ would have unphysical behavior. The quadratic and cubic force constants, $k_2(r)$and $k_3(r)$, as well as the equilibrium bond angles $\theta_0(r)$ depend parametrically on the O−H bond length. The parametric dependence of the equilibrium bond angle on the O−H bond length is fitted with a switching function:

$$\cos\theta_0(r) = \cos\theta_1 + \frac{1 + \tan a(r - r_0)}{2}(\cos\theta_2 - \cos\theta_1) \quad (12)$$

where cos θ_1, cos θ_2, a, and r_0 are adjustable parameters. The force constants were fitted with linear combinations of Gaussian functions:

$$k_i(r) = \sum_{j=1}^{N_{G,i}} A_{i,j}\exp[-\alpha_{i,j}(r - r_{i,j})^2] \quad (13)$$

where $N_{G,i}$ is the number of Gaussian functions used to fit $k_i(r)$. Contour plots of the calculated and fitted bending potentials are compared in Figure 3; they are in good agreement.

The H−O−C−H torsion potential was calculated for $\varphi_{HOCH} = 0$−$180°$ with a step size of 10° for $r = 0.65$−4.0 Å. Contour plots of the torsion energy profiles along the O−H dissociation are shown in Figure 4a. The H−O−C−H torsion energy reaches its minimum for $\varphi_{HOCH} = 180°$, 60°, and by symmetry, −60°. It is interesting that the torsion barrier increases first as the O−H bond length increases, reaching its maximum around 1.7 Å, and decreases as the O−H bond length increases further; this nonmonotonic trend is understandable since in the two limits of r_{OH} equal to 0 and to infinity, the barrier should be zero. A cosine function was used to fit the torsion energy

dx.doi.org/10.1021/ct401074s | J. Chem. Theory Comput. XXXX, XXX, XXX−XXX

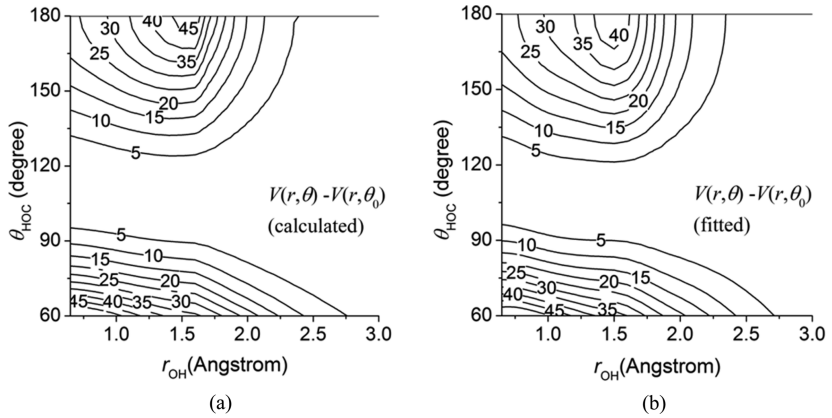

Figure 3. Contour plots of calculated and fitted H−O−C bending potential energies (in kcal/mol) along the O−H dissociation path (Note that θ_0 is a function of r_{OH}). All internal coordinates except r_{OH} and θ_{HOC} are held constant at their reference values for this figure.

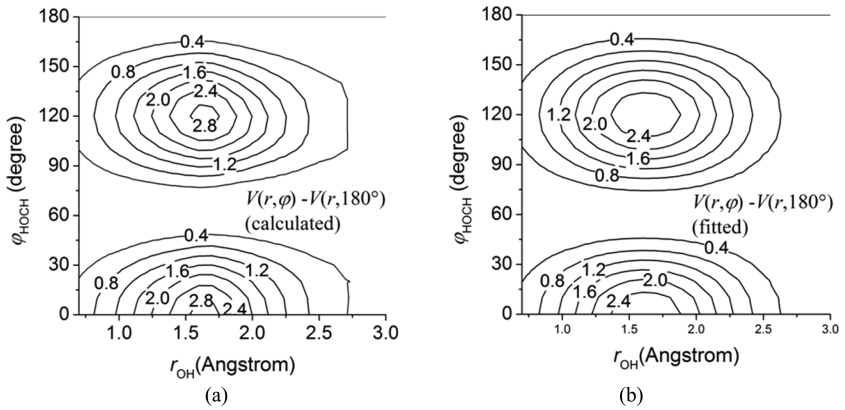

Figure 4. Contour plots of calculated and fitted H−O−C−H torsional potential energies (in kcal/mol) along the O−H dissociation path. All internal coordinates except r_{OH} and φ_{HOCH} are relaxed in the calculation of this secondary torsion.

$$V_{tor}^{[2]}(\varphi|r) = V_3(r)[1 - \cos 3(\varphi - \varphi_0)] \quad (14)$$

The parametric dependence of torsion barrier $V_3(r)$ on O−H bond length is fitted with linear combination of Gaussian functions:

$$V_3(r) = \sum_{i=1}^{N_G} A_i \exp[-\alpha_i (r - r_i)^2] \quad (15)$$

A contour plot of the fitted torsion energy is shown in Figure 4b. It reproduces the calculated result in Figure 4a very well. Unlike the other terms in the primary and secondary potentials, the parameters in the secondary torsion were explained with relaxed structures, that is, all internal coordinates except r_{OH} and φ_{HOCH} are relaxed in the calculation.

Now we turn to $V^{[3]}$, which depends on tertiary coordinates and depends parametrically on r_{OH}. We optimized CH_3OH and CH_3O to obtain their equilibrium geometric parameters and force constant matrices (Hessians) needed for the molecular mechanics force fields in the tertiary subspace. In addition to CH_3OH and CH_3O, three more structures were partially optimized with fixed O−H bond lengths (r_{OH} = 1.5, 2.0, and 3.0 Å) to obtain the equilibrium geometric parameters and force constants matrices along the dissociation path. Five anchor structures were used to describe the distortion of tertiary coordinates along the O−H bond dissociation path. Four of these structures were the optimized structure with r_{OH} = 0.966 Å and the partially optimized structures with r_{OH} = 1.5, 2.0, and 3.0 Å; the fifth was an anchor structure at r_{OH} = 5.0 Å, taken to have the energy and force constant matrix of CH_3O. Since there are no soft torsions in the tertiary coordinates for this system, eq 6 was used to describe distortions of tertiary coordinates in the vicinity of each anchor structure, and eq 2 was used to describe the tertiary potential all along the dissociation path.

As specified above, redundant internal coordinates are used as the tertiary coordinates for the construction of APRP PES. However, to test the performance of APRP, one needs to work with nonredundant coordinates that uniquely define a structure. A set of nonredundant internal coordinates are chosen as the following:

S_1–S_4: r_{12}, r_{13}, r_{14}, r_{15}

S_5: r_{56}

S_6: $(\theta_{314} + \theta_{213} + \theta_{214} - \theta_{215} - \theta_{315} - \theta_{415})/\sqrt{6}$

S_7: $(2\theta_{314} - \theta_{213} - \theta_{214})/\sqrt{6}$

S_8: $(\theta_{213} - \theta_{214})/\sqrt{2}$

S_9: $(2\theta_{215} - \theta_{315} - \theta_{415})/\sqrt{6}$

S_{10}: $(\theta_{315} - \theta_{415})/\sqrt{2}$

S_{11}: θ_{651}

dx.doi.org/10.1021/ct401074s | J. Chem. Theory Comput. XXXX, XXX, XXX−XXX

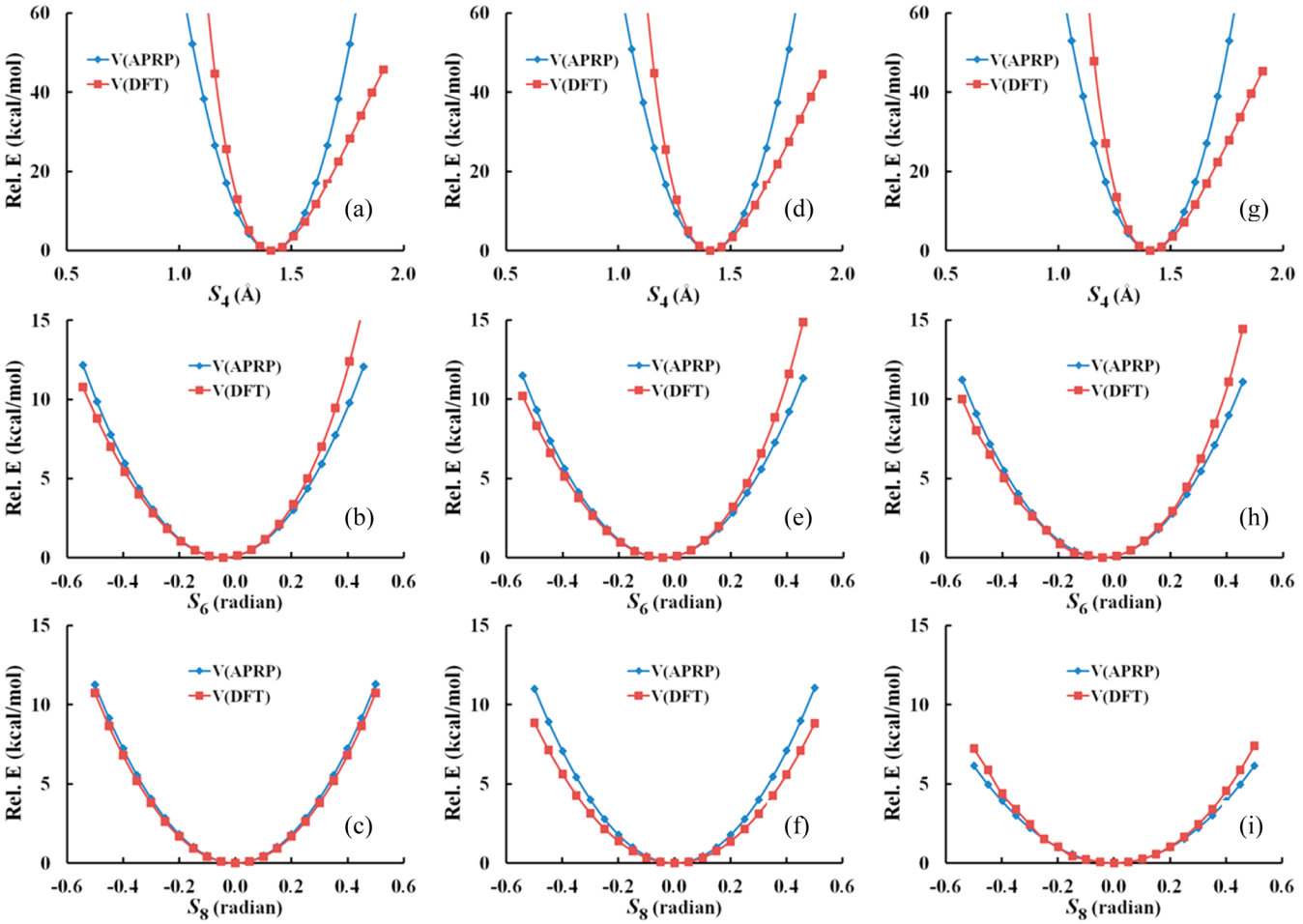

Figure 5. Slected slices along the degrees of freedom S_4, S_6, and S_8 (From left to right $r_{OH} = r_e$, 2.0, and 4.0 Å).

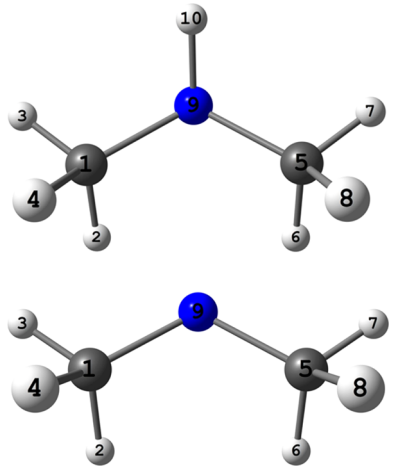

Figure 6. Geometries of $HN(CH_3)_2$ (top, C_s) and $N(CH_3)_2$ (bottom, C_{2V}).

S_{12}: φ_{6512}

In this choice of nonredundant internal coordinates, S_5 is the reaction coordinate equal to the O−H bond length, S_{11} and S_{12} are the H−O−C bending and H−O−C−H torsion included in the secondary coordinates. S_1−S_4 are bond lengths in tertiary coordinates, and S_6-S_{10} are linear combinations of bond angles used to construct nonredundant internal coordinates as suggested by Pulay and co-workers.[59] Three slices of the potential energy curves along the nonreduandant internal coordinates, S_4, S_6, and S_8, are shown in Figure 5 for three different O−H bond lengths ($r_{OH} = r_e$, 2.0, and 4.0 Å).

Figure 5a, d, and g show the comparison of DFT calculated potential energy curves and APRP potential energy curves along the C−O bond stretching. They agree with each other near the equilibrium bond distance, but the APRP curves are too replusive for stretched bonds and not repulsive enough for compressed bonds, which is a typical result of bond stretrch anharmonicity. Model potentials such as Morse potential or

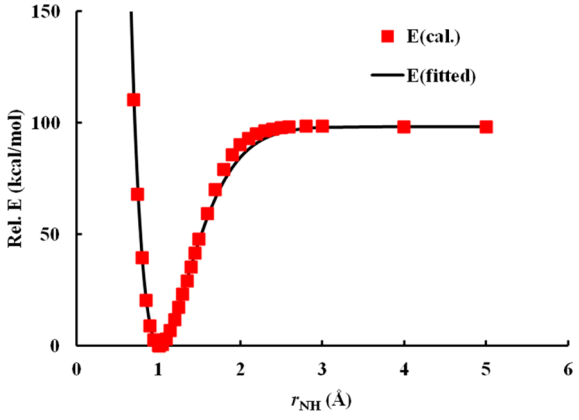

Figure 7. Varshni potential to describe the N−H bond dissociation in $HN(CH_3)_2$.

dx.doi.org/10.1021/ct401074s | J. Chem. Theory Comput. XXXX, XXX, XXX−XXX

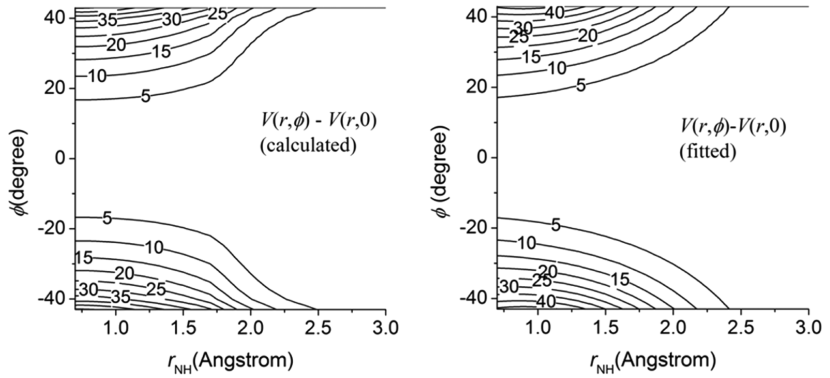

Figure 8. Contour plots of calculated and fitted H−N−C bending potential energies (in kcal/mol) along the N−H dissociation path.

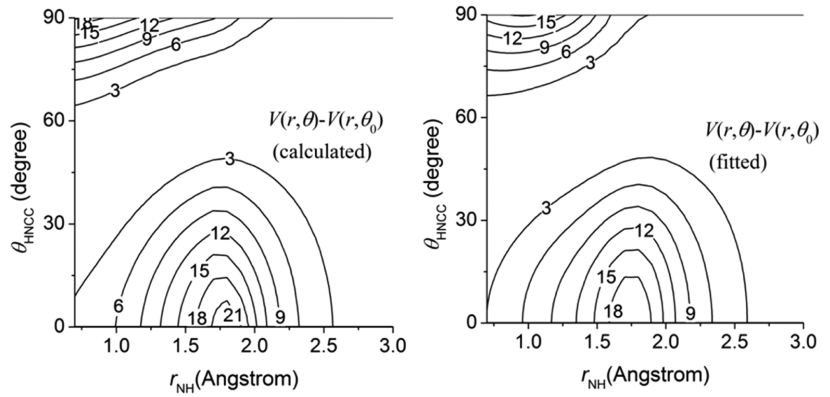

Figure 9. Contour plots of calculated and fitted H−N−C−C out-of-plane potential energies (in kcal/mol) along the N−H dissociation (Note that θ_0 is a function of r_{NH}).

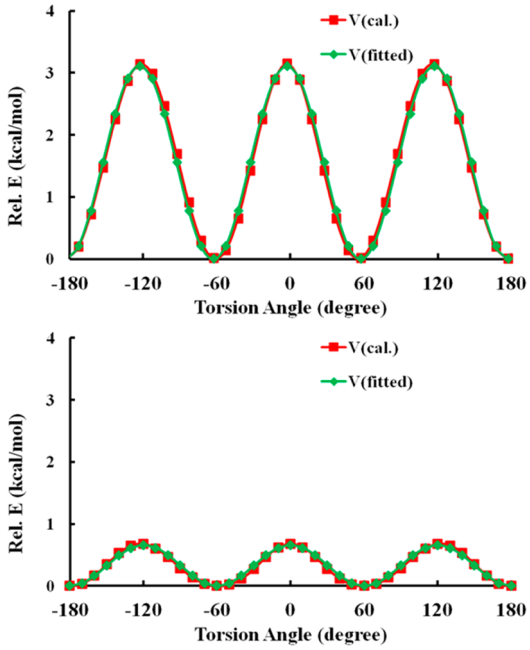

Figure 10. Calculated and fitted H−C−N−C torsion profiles of $HN(CH_3)_2$ (top) and $N(CH_3)_2$ (bottom).

Varshni potential can be used for bond stretching if more accurate descriptions are needed. However, in the photodissociation reaction under consideration, the displacements along these coordiantes are expected to be small at the energies of interest, so the harmonic approximation should be adequate.

The comparison of DFT and APRP potential energy curves along S_6 and S_8 are shown in Figure 5b and c, e and f, and h and i, for $r_{OH} = r_e$, 2.0, and 4.0 Å, respectively. They agree well with each other in all cases. We note that no information (neither equilibrium geometric parameters nor Hessians) were input to the fit at r_{OH} = 4.0 Å, but APRP nevertheless describes the potential energy curves quite well for this O−H distance.

3.2. $(H_3C)_2NH \rightarrow (H_3C)_2N + H$. The reference structure for the parametrization of the primary and secondary potentials is taken to be the equilibrium geometry of $(H_3C)_2NH$. The $(H_3C)_2NH$ molecule has C_s symmetry. When the H atom is dissociated, the $(H_3C)_2N$ radical has C_{2v} symmetry. The optimized geometries and atomic labeling are shown in Figure 6. To treat the N−H bond dissociation, the N−H distance (which may be called either r_{NH} or r_{9-10}) was chosen as the reaction coordinate; and the bends and out-of-plane bend that involve the dissociating H are chosen as secondary coordinates; in particular the secondary coordinates are two H−N−C bond angles θ_{HNC} (θ_{10-9-1} and θ_{10-9-5}) and the H−N−C−C out-of-plane bend θ_{HNCC} ($\theta_{10-9-1-5}$). These three coordinates cannot all change independent, so we used θ_{HNCC} and a linear combination, $\phi = (1/\sqrt{2})(\theta_{10-9-1} - \theta_{10-9-5})$, of the other two coordinates as nonredundant coordinates for fitting V[2]. The other 8 bond lengths, 13 bond angles, and 6 torsions, in which the dissociated H atom (H_{10}) is not involved, were chosen as tertiary coordinates.

The Varshni model potential, eq 10, was used to fit the N−H dissociation curve in $(H_3C)_2NH$. The calculated and fitted N−H dissociation curves are shown in Figure 7; they agree well.

dx.doi.org/10.1021/ct401074s | J. Chem. Theory Comput. XXXX, XXX, XXX−XXX

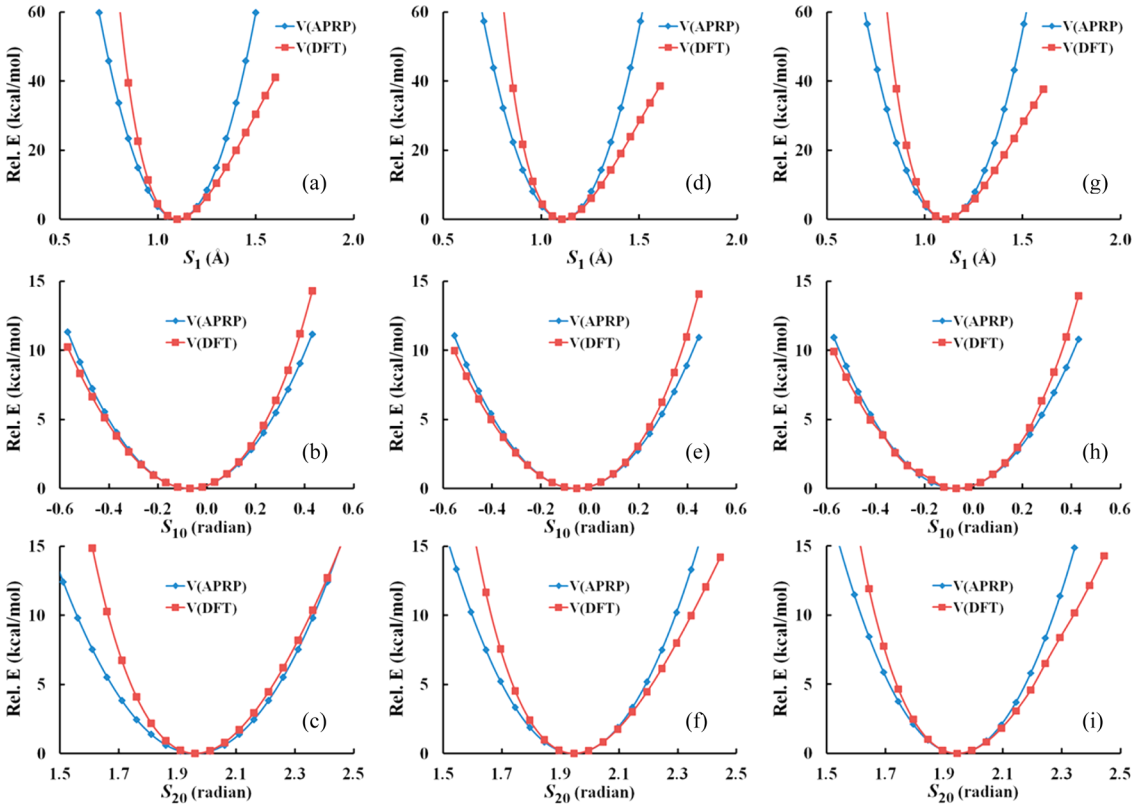

Figure 11. Slices of the potential surface along the degrees of freedom S_1, S_{10}, and S_{20}. (From left to right, $r_{NH} = r_e$, 2.0, and 4.0 Å.).

A scan was performed for r = 0.7 Å to 4.0 Å and $\phi = -43°$ to 43° with other coordinates constrained to their values at the $(H_3C)_2NH$ equilibrium geometry. The calculated H−N−C bending potential energies along the N−H dissociation are shown in Figure 8a. The following functional form was chosen to fit the H−N−C bending potential energies

$$V_{bend}^{[2]}(\phi|r) = k_2(r)\phi^2 + k_4(r)\phi^4 \quad (16)$$

The cubic force constant, $k_3(r)$, is zero as a result of our definition of ϕ. The quadratic and quartic force constants, $k_2(r)$ and $k_4(r)$, depend parametrically on the N−H bond length, and they were fitted with linear combinations of Gaussian functions as shown in eq 13. A contour plot of the fitted H−N−C bending potential energies along the N−H dissociation is shown in Figure 8b, and it reproduces the main features of the calculated one in Figure 8a, where they are seen to agree well.

The H−N−C−C out-of-plane bend potentials are calculated for θ_{HNCC} = 0−90° and r = 0.7−4.0 Å. Figure 9a shows 2D contour plots of the out-of-plane bending potential energy profiles along the N−H dissociation. Equation 11 was used to fit this potential, and a 2D contour plot of the fitted potential is shown in Figure 9b.

The tertiary potential for $(H_3C)_2NH$ was obtained by performing optimization and frequency analysis of $(H_3C)_2NH$ and $(H_3C)_2N$, and partial optimization and frequency analysis of three other anchor structures with r_{NH} = 1.5, 2.0, and 3.0 Å. The bond stretches and bond angle bends were treated with eq 6 as in the case of CH_3OH. Since $(H_3C)_2NH$ has soft torsions, in particular HCNC torsions, in the tertiary subspace, eq 7 was used for this molecule although it was not needed for methanol. The HCNC torsion potentials of $(H_3C)_2NH$ at the five anchor structures were fitted with the following functional form

$$V_a^{MM}(\varphi) = V_i^{[a]}[1 - \cos 3(\varphi - \varphi_0)] \quad (17)$$

where a is the index of anchor structures. The calculated and fitted torsion potentials in $(H_3C)_2NH$ and $(H_3C)_2N$ are shown in Figure 10.

Again, to test the performance of APRP for tertiary coordinates, a set of nonredundant internal coordinates was chosen for $(H_3C)_2NH$. Potential energy curves along three selected coordinates (S_1, S_{10}, and S_{20}) at $r_{NH} = r_e$, 2.0, and 4.0 Å were calculated with both DFT and APRP and are shown in Figure 11. The definition of nonredundant internal coordinates is described in detail in the Supporting Information and the potential dependence on the coordinates is shown for only three selected coordinates:

S_1: r_{1-2}

S_{10}: $(\theta_{3-1-4} + \theta_{2-1-3} + \theta_{2-1-4} - \theta_{2-1-9} - \theta_{3-1-9} - \theta_{4-1-9})/\sqrt{6}$

S_{20}: θ_{1-9-5}

As in the case of CH_3OH, the APRP potential energy curves agree well with the DFT ones near the equilibrium bond lengths but fail to describe the anhormonicity for large bond stretches. The APRP potential energy curves along bond angle coordinates reproduce the DFT ones well, both for anchor structures and for nonanchor structures. These plots show that APRP is able to describe the potential well for small distortions along the bond dissociation coordinate by interpolating between anchor structures.

dx.doi.org/10.1021/ct401074s | J. Chem. Theory Comput. XXXX, XXX, XXX−XXX

3.3. Subroutines. The two potential energy functions obtained in the present study are available (free) online in the POTLIB library.[60,61]

4. CONCLUDING REMARKS

By combining model potentials and internal coordinate force fields, we have developed a new scheme called anchor points reactive potential (APRP) to fit high-dimensional PESs. Analytic gradients of APRP PESs can be easily implemented for dynamic studies by using Wilson's B matrix. We illustrated the APRP method by applying it to construct the full dimensional PESs of CH_3OH and $(H_3C)_2NH$ to describe the X−H (X = O or N) bond breaking processes. It would be impractical to fit these potential energy surfaces with conventional PES fitting methods, but the present method is straightforwardly applicable and indeed would be applicable to much larger systems as well. The new method may be considered to be an extension of some previous methods[29,30,62,63] for fitting analytical potentials based in whole or in part on quantum mechanical Hessians, but those methods were developed for representing the potential in the vicinity of a single equilibrium structure, and the present method is designed for reactive potentials. It may also be compared to Shepard interpolation,[64,65] but it is more systematic in its design.

Although these examples involve only bond breaking, the method could be extended in a straightforward way to isomerization processes in which bonds are both broken and formed. Another generalization is that, although the APRP is applied here to Born−Oppenheimer processes occurring on the ground electronic state, it could also be applied to electronically nonadiabatic processes of large molecules, such as light-induced DNA damage or photodissociation. The method would be especially well suited to fitting diabatic PESs for photodissociation, such as those recently reported for phenol.[66]

■ ASSOCIATED CONTENT

Ⓢ Supporting Information

Details of the functional forms used for fitting and the optimized fitting parameters, the definitions of internal coordinates, and the Hessians at anchor structures. This material is available free of charge via the Internet at http://pubs.acs.org.

■ AUTHOR INFORMATION

Corresponding Author

*E-mail: truhlar@umn.edu.

Notes

The authors declare no competing financial interest.

■ ACKNOWLEDGMENTS

This material is based upon work supported by the U.S. Department of Energy, Office of Basic Energy Sciences, under grant No. DE-SC0008666 (K.R.Y. and D.G.T.) and grant No. DE-FG02-86ER13579 (X.X. and D.G.T.).

■ REFERENCES

(1) Truhlar, D. G.; Steckler, R.; Gordon, M. S. Potential energy surfaces for polyatomic reaction dynamics. *Chem. Rev.* **1987**, *87*, 217−236. Schatz, G. C. The analytic representation of electronic potential-energy surfaces. *Rev. Mod. Phys.* **1989**, *61*, 669−688.

(2) Hollebeek, T.; Ho, T.-S.; Rabitz, H. Constructing multidimensional molecular potential energy surface from ab initio data. *Annu. Rev. Phys. Chem.* **1990**, *50*, 537−570.

(3) Fernández-Ramos, A.; Miller, J. A.; Klippenstein, S. J.; Truhlar, D. G. Modeling the kinetics of bimolecular reactions. *Chem. Rev.* **2006**, *106*, 4518−4584.

(4) Albu, T. V.; Espinosa-García, J.; Truhlar, D. G. Computational chemistry of polyatomic reaction kinetics and dynamics: The quest for an accurate CH_5 potential energy surface. *Chem. Rev.* **2007**, *107*, 5101−5132.

(5) Brooks, B. R.; Bruccoleri, R. E.; Olafson, B. D.; States, D. J.; Swaminathan, S.; Karplus, M. CHARMM: A program for macromolecular energy, minimization, and dynamics calculations. *J. Comput. Chem.* **1983**, *4*, 187−217.

(6) MacKerell, A. D., Jr.; Bashford, D.; Bellott, M.; Dunbrack, R. L., Jr.; Evanseck, J. D.; Field, M. J.; Fischer, S.; Gao, J.; Guo, H.; Ha, S.; Joseph-McCarthy, D.; Kuchnir, L.; Kuczera, K.; Lau, F. T. K.; Mattos, C.; Michnick, S.; Ngo, T.; Nguyen, D. T.; Prodhom, B.; Reiher, W. E., III; Roux, B.; Schlenkrich, M.; Smith, J. C.; Stote, R.; Straub, J.; Watanabe, M.; Wiorkiewicz-Kuczera, J.; Yin, D.; Karplus, M. All-atom empirical potential for molecular modeling and dynamics studies of proteins. *J. Phys. Chem. B* **1998**, *102*, 3586−3616.

(7) Mackerell, A. D., Jr.; Feig, M.; Brooks, C. L. Extending the treatment of backbone energetics in protein force fields: Limitations of gas-phase quantum mechanmics in reproducing protein conformational distributions in molecular dynamics simulations. *J. Comput. Chem.* **2004**, *25*, 1400−1415.

(8) Vanommeslaeghe, K.; Hatcher, E.; Acharya, C.; Kundu, S.; Zhong, S.; Shim, J.; Darian, E.; Gubench, O.; Lopes, P.; Vorobyov, I.; Mackerell, A. D., Jr. CHARMM general force filed: A force field for drug-like molecules compatible with the CHARMM all-atom additive biological force fields. *J. Comput. Chem.* **2010**, *31*, 671−690.

(9) Weiner, S. J.; Kollman, P. A.; Nguyen, D. T.; Case, D. A. An all-atom force field for simulations of proteins and nucleic acids. *J. Comput. Chem.* **1986**, *7*, 230−252.

(10) Cornell, W. D.; Cieplak, P.; Bayly, C. I.; Gould, I. R.; Merz, K. M., Jr.; Ferguson, D. M.; Spellmeyer, D. C.; Fox, T.; Caldwell, J. W.; Kollman, P. A. A second generation force field for the simulation of proteins, nucleic acids, and organic molecules. *J. Am. Chem. Soc.* **1995**, *117*, 5179−5197.

(11) Hornak, V.; Abel, R.; Okur, A.; Strockbine, B.; Roitberg, A.; Simmerling, C. Comparison of multiple Amber force fields and development of improved protein backbone parameters. *Protein* **2006**, *65*, 712−725.

(12) Pérez, A.; Marchán, I.; Svozil, D.; Sponer, J.; Cheatham, T. E.; Laughton, C. A.; Orozco, M. Refinement of the AMBER force field for nucleic acids: Improving the description of α/γ conformers. *Biophys. J.* **2007**, *92*, 3817−3829.

(13) Lindorff-Larsen, K.; Piana, S.; Palmo, K.; Maragakis, P.; Klepeis, J. L.; Dror, R. O.; Shaw, D. E. Improved side-chain torsion potentials for the Amber ff99SB protein force field. *Proteins* **2010**, *78*, 1950−1958.

(14) Scott, W. R. P.; Hunenberger, P. H.; Tironi, I. G.; Mark, A. E.; Billeter, S. R.; Fennen, J.; Torda, A. E.; Huber, T.; Kruger, P.; van Gunsteren, W. F. The GROMOS biomolecular simulation program package. *J. Phys. Chem. A* **1999**, *103*, 3596−3607.

(15) Allinger, N. L.; Yuh, Y. H.; Lii, J.-H. Molecular mechanics. The MM3 force field for hydrocarbons. 1. *J. Am. Chem. Soc.* **1989**, *111*, 8551−8566.

(16) Lii, J.-H.; Allinger, N. L. Molecular mechanics. The MM3 force field for hydrocarbons. 2. Vibrational frequencies and thermodynamics. *J. Am. Chem. Soc.* **1989**, *111*, 8566−8575.

(17) Lii, J.-H.; Allinger, N. L. Molecular mechanics. The MM3 force field for hydrocarbons. 3. The van der Waals' potentials and crystal data for aliphatic and aromatic hydrocarbons. *J. Am. Chem. Soc.* **1989**, *111*, 8576−8582.

(18) Kaminski, G.; Duffy, E. M.; Matsui, T.; Jorgensen, W. L. Free energies of hydration and pure liquid properties of hydrocarbons from the OPLS all-atom model. *J. Phys. Chem.* **1994**, *98*, 13077−13081.

(19) Damm, W.; Frontera, A.; Tirado-Rives, J.; Jorgensen, W. L. OPLS all-atom force field for carbohydrates. *J. Comput. Chem.* **1997**, *18*, 1955−1970.
(20) Jorgensen, W. L.; Tirado-Rives, J. Molecular modeling of organic and biomolecular systems using BOSS and MCPRO. *J. Comput. Chem.* **2005**, *26*, 1689−1700.
(21) A.K. Rappe, A. K.; Casewit, C. J.; Colwell, K. S.; Goddard, W. A., III; Skiff, W. M. UFF, a full periodic table force field for molecular mechanics and molecular dynamics simulations. *J. Am. Chem. Soc.* **1992**, *114*, 10024−10035.
(22) Halgren, T. A. Merck molecular force field. I. Basis, form, scope, parameterization, and performance of MMFF94. *J. Comput. Chem.* **1996**, *17*, 490−519.
(23) Halgren, T. A. Merck molecular force field. II. MMFF94 van der Waals and electrostatic parameters for intermolecular interactions. *J. Comput. Chem.* **1996**, *17*, 520−552.
(24) Halgren, T. A. Merck molecular force field. III. Molecular geometries and vibrational frequencies for MMFF94. *J. Comput. Chem.* **1996**, *17*, 553−586.
(25) Halgren, T. A.; Nachbar, R. B. Merck molecular force field. IV. Conformational energies and geometries for MMFF94. *J. Comput. Chem.* **1996**, *17*, 587−615.
(26) Wang, J.; Wolf, R. M.; Caldwell, J. W.; Kollman, P. A.; Case, D. A. Development and testing of a general Amber force field. *J. Comput. Chem.* **2004**, *25*, 1157−1174.
(27) Chen, B.; Siepmann, J. I. Transferable potentials for phase equilibria. 3. Explicit-hydrogen description of normal alkanes. *J. Phys. Chem. B* **1999**, *103*, 5370−5379.
(28) Rai, N.; Siepmann, J. I. Transferable potentials for phase equilibria. 10. Explicit-hydrogen description of substituted benzenes and polycyclic aromatic compounds. *J. Phys. Chem. B* **2013**, *117*, 273−288.
(29) Cacelli, I.; Prampolini, G. Parametrization and validation of intramolecular force fields derived from DFT calculations. *J. Chem. Theory. Comput.* **2007**, *3*, 1803−1817.
(30) Barone, V.; Cacelli, I.; De Mitri, N.; Licari, D.; Monti, S.; Prampolini, G. JOYCE and ULYSSES: Integrated and user-friendly tools for the parameterization of intramolecular force fields from quantum mechanical data. *Phys. Chem. Chem. Phys.* **2013**, *15*, 3736−3751.
(31) Braams, B. J.; Bowman, J. M. Permutationally invariant potential energy surfaces in high dimensionality. *Int. Rev. Phys. Chem.* **2009**, *28*, 577−606.
(32) Bowman, J. M.; Braams, B. J.; Carter, S.; Chen, C.; Czakó, G.; Fu, B.; Huang, X.; Kamarchik, E.; Sharma, A. R.; Shepler, B. C.; Wang, Y.; Xie, Z. Ab-initio-based potential energy surfaces for complex molecules and molecular complexes. *J. Phys. Chem. Lett.* **2010**, *1*, 1866−1874.
(33) Dawes, R.; Thompson, D. L.; Guo, Y.; Wagner, A. F.; Minkoff, M. Interpolating moving least-squares methods for fitting potential energy surfaces: Computing high-density potential energy surface data from low-density ab initio data points. *J. Chem. Phys.* **2007**, *126*, 184108.
(34) Guo, Y.; Tokmakov, I.; Thompson, D. L.; Wagner, A. F.; Minkoff, M. Interpolating moving least-squares methods for fitting potential energy surfaces: Improving efficiency via local approximants. *J. Chem. Phys.* **2007**, *127*, 214106.
(35) Dawes, R.; Thompson, D. L.; Wagner, A. F.; Minkoff, M. Interpolating moving least-squares methods for fitting potential energy surfaces: A strategy for efficient automatic data point placement in high dimensions. *J. Chem. Phys.* **2008**, *128*, 084107.
(36) Brenner, D. W.; Shenderova, O. A.; Harrison, J. A.; Stuart, S. J.; Ni, B.; Sinnott, S. B. *Condens. Matter* **2002**, *14*, 783−802.
(37) Brenner, D. W.; Shenderova, O. A.; Schall, J. D.; Areshkin, D. A.; Adiga, S.; Harrsion, J. A.; Stuart, S. J. In *Handbook of Nanoscience, Engineering, and Technology*; Goddard, W. A. III, Brenner, D. W., Lyshevski, S. E., Iafrate, G. J., Eds.; CRC Press: Boca Raton, FL, 2003; Chapter 24.
(38) van Duin, A. C. T.; Dasgupta, S.; Lorant, F.; Goddard, W. A. ReaxFF: A reactive force field for hydrocarbons. *J. Phys. Chem. A* **2001**, *105*, 9396−9409.
(39) Kulkarni, A.; Truhlar, D. G.; Goverapet Srinivasan, S.; van Duin, A.; Norman, P.; Schwartzentruber, T. Oxygen interactions with silica surfaces: Coupled cluster and density functional investigation and the development of a new ReaxFF potential. *J. Phys. Chem. C* **2013**, *117*, 258−269.
(40) Zhao, M.; Iron, M. A.; Staszewski, P.; Schultz, N. E.; Valero, R.; Truhlar, D. G. Valence−bond order (VBO): A new approach to modeling reactive potential energy surfaces for complex systems, materials, and nanoparticles. *J. Chem. Theory Comput.* **2009**, *5*, 594−604.
(41) Gao, J. Methods and applications of combined quantum mechanical and molecular mechanical potentials. *Rev. Comp. Chem.* **1996**, *7*, 119−185.
(42) Monard, G.; Merz, K. M., Jr. Combined quantum mechanical/molecular mechanical methodologies applied to biomolecular systems. *Acc. Chem. Res.* **1999**, *32*, 904−911.
(43) Gao, J.; Truhlar, D. G. Quantum mechanical methods for enzyme kinetics. *Annu. Rev. Phys. Chem.* **2002**, *53*, 467−505.
(44) Friesner, R. A.; Guallar, V. Ab initio quantum chemical and mixed quantum mechanics/molecular mechanics (QM/MM) methods for studying enzymatic catalysis. *Annu. Rev. Phys. Chem.* **2005**, *56*, 389−427.
(45) Lin, H.; Truhlar, D. G. QM/MM: What have we learned, where are we, and where do we go from here? *Theor. Chem. Acc.* **2007**, *117*, 185−199.
(46) Hu, H.; Yang, W. Free energies of chemical reactions in solution and in enzymes with ab initio quantum mechanics/molecular mechanics methods. *Annu. Rev. Phys. Chem.* **2008**, *59*, 573−601.
(47) Senn, H. M.; Thiel, W. QM/MM methods for biomolecular systems. *Angew. Chem., Int. Ed.* **2009**, *48*, 1198−1229.
(48) Chakraborty, A.; Zhao, Y.; Lin, H.; Truhlar, D. G. Combined valence bond-molecular mechanics potential-energy surface and direct dynamics study of rate constants and kinetic isotope effects for the H + C_2H_6 reaction. *J. Chem. Phys.* **2006**, *124*, 044315.
(49) Wilson, E. B. Jr.; Decius, J. C.; Cross, P. C. *Molecular Vibrations: The Theory of Infrared and Raman Vibrational Spectra*; McGraw-Hill: London, 1955.
(50) Williams, I. H. Torsional internal coordinates in normal coordinate calculations. *J. Mol. Spectrosc.* **1977**, *66*, 288−301.
(51) McIntosh, D. F.; Michaelian, K. H.; Wilson, G. F. Matrix-method of vibrational analysis. 2. Theory and worked examples of the construction of the B-matrix. *Can. J. Spectrosc.* **1979**, *24*, 65−74.
(52) Frisch, M. J.; Trucks, G. W.; Schlegel, H. B.; Scuseria, G. E.; Robb, M. A.; Cheeseman, J. R.; Scalmani, G.; Barone, V.; Mennucci, B.; Petersson, G. A.; Nakatsuji, H.; Caricato, M.; Li, X.; Hratchian, H. P.; Izmaylov, A. F.; Bloino, J.; Zheng, G.; Sonnenberg, J. L.; Hada, M.; Ehara, M.; Toyota, K.; Fukuda, R.; Hasegawa, J.; Ishida, M.; Nakajima, T.; Honda, Y.; Kitao, O.; Nakai, H.; Vreven, T.; Montgomery, Jr., J. A.; Peralta, J. E.; Ogliaro, F.; Bearpark, M.; Heyd, J. J.; Brothers, E.; Kudin, K. N.; Staroverov, V. N.; Kobayashi, R.; Normand, J.; Raghavachari, K.; Rendell, A.; Burant, J. C.; Iyengar, S. S.; Tomasi, J.; Cossi, M.; Rega, N.; Millam, J. M.; Klene, M.; Knox, J. E.; Cross, J. B.; Bakken, V.; Adamo, C.; Jaramillo, J.; Gomperts, R.; Stratmann, R. E.; Yazyev, O.; Austin, A. J.; Cammi, R.; Pomelli, C.; Ochterski, J. W.; Martin, R. L.; Morokuma, K.; Zakrzewski, V. G.; Voth, G. A.; Salvador, P.; Dannenberg, J. J.; Dapprich, S.; Daniels, A. D.; Farkas, Ö.; Foresman, J. B.; Ortiz, J. V.; Cioslowski, J.; Fox, D. J. *Gaussian 09*, Revision D.01, Gaussian, Inc.: Wallingford, CT, 2009.
(53) Zhao, Y.; Truhlar, D. G. The M06 suite of density functionals for main group thermochemistry, thermochemical kinetics, noncovalent interactions, excited states, and transition elements: two new functionals and systematic testing of four M06-class functionals and 12 other functionals. *Theor. Chem. Acc.* **2008**, *120*, 215−241.
(54) (a) Hehre, W. J.; Ditchfield, R.; Pople, J. A. Self-consistent molecular orbital methods. XII. Further extensions of Gaussian-type basis sets for use in molecular orbitals studies of organic molecules. *J.*

Chem. Phys. **1972**, *56*, 2257−2261. (b) Hariharan, P. C.; Pople, J. A. The influence of polarization functions on molecular orbital hydrogenation energies. *Theoretica. Chimica. Acta.* **1973**, *3*, 213−222. (c) Clark, T.; Chandrasekhar, J.; Spitznagel, G. W.; Schleyer, P. v. R. Efficient diffuse function-augmented basis sets for anion calculations. III. The 3-21+G basis set for first-row elements Li-F. *J. Comput. Chem.* **1983**, *4*, 294−301.

(55) Bersuker, I. B. Modern aspects of the Jahn−Teller effect: Theory and application to molecular problem. *Chem. Rev.* **2001**, *101*, 1067−1114.

(56) Varshni, Y. P. Comparative study of potential energy functions for diatomic molecules. *Rev. Mod. Phys.* **1957**, *29*, 664−682; *Erratum* **1959**, *31*, 839−839.

(57) Steele, D.; Lippincott, E. R.; Vanderslice, J. T. Comparative study of empirical internuclear potential functions. *Rev. Mod. Phys.* **1962**, *34*, 239−251.

(58) Brown, F. B.; Truhlar, D. G. Dissociation potential for breaking a C−H bond in methane. *Chem. Phys. Lett.* **1985**, *113*, 441−446.

(59) Pulay, P.; Fogarasi, G.; Pang, F.; Boggs, J. E. Systematic ab initio gradient calculation of molecular geometries, force constants, and dipole moment derivatives. *J. Am. Chem. Soc.* **1979**, *101*, 2550−2560.

(60) Duchovic, R. J.; Volobuev, Y. L.; Lynch, G. C.; Allison, T. C.; Corchado, J. C.; Truhlar, D. G.; Wagner, A. F.; Garrett, B. C. POTLIB 2001: A potential energy surface library for chemical systems. *Comput. Phys, Commun.* **2004**, *144*, 169−187; *Erratum* **2004**, *156*, 319−322.

(61) Duchovic, R. J.; Volobuev, Y. L.; Lynch, G. C.; Jasper, A. W.; Truhlar, D. G.; Allison, T. C.; Wagner, A. F.; Garrett, B. C.; Espinosa-Garcia, J.; Corchado, J. C. *POTLIB: An Online Library of Potential Energy Surfaces*. http://comp.chem.umn.edu/potlib/ (accessed Dec. 11, 2013).

(62) Pongor, G.; Fogarezi, G.; Boggs, J. E.; Pulay, P. Theoretical prediction of vibrational spectra: The out-of-plane force field and vibrational spectra of pyridine. *J. Mol. Spectrosc.* **1985**, *114*, 445−453.

(63) Dasgupta, S.; Brameld, K. A.; Fan, C.-F.; Goddard, W. A., III. Ab initio derived spectroscopic quality force fileds for molecular modeling and dynamics. *Spectrochim. Acta* **1997**, *53*, 1347−1363.

(64) Thompson, K. C.; Jordan, M. J. T.; Collins, M. A. Polyatomic molecular potential energy surfaces by interpolation in local internal coordinates. *J. Chem. Phys.* **1998**, *108*, 8302−8316.

(65) Tishchenko, O.; Truhlar, D. G. Gradient-based multiconfiguration shepard interpolation for generating potential energy surfaces for polyatomic reactions. *J. Chem. Phys.* **2010**, *132*, 084109.

(66) Xu, X.; Yang, K. R.; Truhlar, D. G. Diabatic molecular orbitals, potential energies, and potential energy surface coupling by fourfold for photodissociation of phenol. *J. Chem. Theory Comput.* **2013**, *9*, 3612−3625.